Suppressed Stark shift of helical edge states in topological-insulator quantum dots

Dingyang Liu,[1] Shu-Hui Zhang,[2,1] Yongwei Huang,[3] Jun Li,[4] Jinxian Qu,[1] and Wen Yang[1,*]

[1]*Beijing Computational Science Research Center, Beijing 100193, China*

[2]*College of Science, Beijing University of Chemical Technology, Beijing 100029, China*

[3]*SKLSM, Institute of Semiconductors, Chinese Academy of Sciences, P.O. Box 912, Beijing 100083, China*

[4]*Department of Physics, Semiconductor Photonics Research Center, Xiamen University, Xiamen 361005, China*

(Received 3 July 2018; revised manuscript received 7 December 2018; published 27 December 2018)

We study the stability of the electronic states in circular two-dimensional topological-insulator quantum dots against electric perturbations, as quantified by the susceptibility χ of the Stark shift $\Delta E = \chi F^2/2$ of each energy level due to a small electric field F. We find the typical susceptibility $\chi_{\text{edge}} \sim 1$ meV/(mV/nm)^2 for edge states is 4 orders of magnitude smaller than $\chi_{\text{bulk}} \sim 10^4$ meV/(mV/nm)^2 for normal bulk states. We show that the origin of this strong stability of the edge states is the equidistance nature of the edge states, which follows from the linear dispersion of the one-dimensional edge channel. Therefore, we expect this strong stability to be a general feature for edge states in relatively large topological-insulator quantum dots. This finding identifies a new physical mechanism for protecting the edge states against electrical perturbations, which may be relevant to the applications of these edge states in quantum technologies.

DOI: 10.1103/PhysRevB.98.245310

I. INTRODUCTION

An insulating energy gap in the bulk along with gapless edge states on the boundary is a hallmark of the (two-dimensional) topological insulator (TI) [1–12]. At each boundary, the two counterpropagating helical (i.e., with spin-velocity locking) edge states form Kramers pairs. These helical edge states are robust against elastic backscattering by nonmagnetic impurities [13–19] and hence give rise to quantized edge conductance—a widely used experimental fingerprint of TIs [5,20–29], which has motivated many proposals for electronic devices [30–37]. In particular, the discrete helical edge states of TI quantum dots (QDs) [38,39] are attracting growing interest [40–49] for potential applications in quantum memory [38], quantum computation [39,50], entangled terahertz photons emission [51], and other key functions in nanoelectronics [52]. However, external perturbations/noises may modify the optical selection rules [53–56] and broaden the energy levels [57,58] of the TI QD. The level broadening effect is especially harmful for the applications of TI QDs in quantum memory [38], quantum computation [39], and entangled terahertz photon emission [51], which rely heavily on the long lifetime of the edge states. Therefore, it is important to investigate the stability of these edge states against electrical perturbations [59], which is common in the solid-state environment.

In this work, we calculate the second-order electrical susceptibility χ for the eigenstate of circular TI QDs, defined via its Stark shift $\Delta E = \chi F^2/2$ induced by an electric field F, as a figure of merit for its stability against external electric perturbations: the smaller the susceptibility $|\chi|$, the more stable the eigenstate. Surprisingly, we find that the typical susceptibility $\chi_{\text{edge}} \sim 1$ meV/(mV/nm)^2 of edge states localizing at the edge of the TI QD is 4 orders of magnitude smaller than the typical susceptibility $\chi_{\text{bulk}} \sim 10^4$ meV/(nV/nm)^2 of normal bulk states localizing at the interior of the TI QD. Our analysis shows that this strong stability of the edge states originates from two essential ingredients: (i) The edge states are spatially separated from the bulk states, so that the contributions to the Stark shift of an edge state due to its coupling to the bulk states are strongly suppressed. (ii) The edge states are nearly equidistant in energy [38,41], so that the contributions to the Stark shift of an edge state due to its coupling to other edge states are strongly canceled. Our work identifies the equidistance nature of the helical edge states as a new physical mechanism for protecting the helical edge states against electrical perturbations in relatively large TI QDs. This may be relevant to the applications of these edge states in quantum information processing [38,39] and entangled terahertz photon emission [51].

The rest of this paper is organized as follows: In Sec. II, we provide explicit analytical expressions to demonstrate the robust, equidistant nature of these edge states. In Sec. III, we demonstrate that this equidistant nature in turn strongly suppresses the Stark shift of the edge states. In Sec. IV, we summarize our findings.

II. EQUIDISTANT EDGE STATES IN TI QUANTUM DOTS

The energy spectrum of a circular two-dimensional TI QD has been discussed in many works [38,40–42,47,49,59]. Previous studies [38,40,41] show that when the QD is sufficiently large, the edge-state energy levels tends to be equidistant, but a quantitative and explicit analytical expression is still lacking. Since the equidistance is the key to the stability of the edge states, we first address this issue in this section.

*wenyang@csrc.ac.cn

We adopt the Bernevig-Hughes-Zhang (BHZ) model [4,8,60,61], relevant to HgTe/CdTe and type-II InAs/GaSb/AlSb quantum wells, to describe the two-dimensional TIs in the xy plane. In the Bloch basis $|e,\uparrow\rangle$, $|hh,\uparrow\rangle$ and $|e,\downarrow\rangle \equiv \hat{\theta}|e,\uparrow\rangle$, $|hh,\downarrow\rangle \equiv \hat{\theta}|hh,\uparrow\rangle$ (with $\hat{\theta}$ the time-reversal operator), the electronic states of a circular TI QD are determined by the 4×4 $\mathbf{k}\cdot\mathbf{p}$ Hamiltonian diag$\{\mathbf{H},\mathbf{H}^*\}$ subjected to the hardwall boundary condition at the QD edge. The 2×2 spin-up block is

$$\mathbf{H} \equiv \begin{bmatrix} M - B_+\hat{k}^2 & A\hat{k}_+ \\ A\hat{k}_- & -M + B_-\hat{k}^2 \end{bmatrix}, \tag{1}$$

where $\hat{\mathbf{k}} \equiv (\hat{k}_x,\hat{k}_y) \equiv (-i\partial/\partial x, -i\partial/\partial y)$ is the in-plane momentum operator, $\hat{k}^2 \equiv \hat{k}_x^2 + \hat{k}_y^2$, $\hat{k}_+ \equiv \hat{k}_x \pm i\hat{k}_y$, and $B_\pm = B \pm D$. The spin-down block $\mathbf{H}^*$ is the time-reversal (or equivalently, complex conjugate since $\hat{\theta}\hat{\mathbf{k}}\hat{\theta}^{-1} = \hat{\mathbf{k}}^* = -\hat{\mathbf{k}}$) of the spin-up block, so the total Hamiltonian is invariant under time reversal. The BHZ model describes a trivial (topological) insulator when $MB < 0$ ($MB > 0$). For HgTe/CdTe quantum wells, A, B, D, and M can be tuned by the well thickness [8,22]. Usually, B is taken to be negative, so $M > 0$ ($M < 0$) denotes the trivial (topological) insulator phase. Here, to keep the generality of our discussions, we do not make this assumption. Due to the time-reversal invariance of the total Hamiltonian, the spin-up and spin-down eigenstates of the TI QD form Kramers pairs, i.e., given a spin-up eigenstate $[F_1(\mathbf{r}), F_2(\mathbf{r})]^T$ with eigenenergy E, its time reversal $[F_1^*(\mathbf{r}), F_2^*(\mathbf{r})]^T$ gives a spin-down eigenstate with the same eigenenergy E. Therefore, in the rest of this paper, we consider only the spin-up block.

Two methods have been widely used to calculate the electronic structure of semiconductor nanostructures in the literature: the basis expansion method and the mode-matching method [62,63]. In previous works on TI QDs, both the basis expansion method [38,41,46,48,59] and the mode-matching method [39,40,44,47,49] have been used to yield convergent results for the energy spectrum and wave function. Here we give the key results of the mode-matching method [40,47,49], leaving the detailed derivations in Appendix A. The first step is to find all the linearly independent bulk eigenstates, i.e., solutions to the Schrödinger equation

$$\mathbf{H}|\psi\rangle = E|\psi\rangle, \tag{2}$$

for the TI bulk material. The second step is to express the QD eigenstate as a linear combination of these bulk eigenstates and then impose the hardwall boundary condition at the QD edge. This determines the allowed QD eigenenergies E as solutions to the transcendental equation [40,47,49]

$$\frac{(M-E)/(k_+B_+) - k_+}{(M-E)/(k_-B_+) - k_-} = \frac{J_m(k_+R)/J_{m-1}(k_+R)}{J_m(k_-R)/J_{m-1}(k_-R)}, \tag{3}$$

where R is the QD radius, $J_m(x)$ is the Bessel function of the mth order, $k_\pm(E) = [-F(E) \pm \sqrt{F^2(E) - (M^2-E^2)/(B_+B_-)}]^{1/2}$, and $F(E) \equiv [A^2 - 2(MB+DE)]/(2B_+B_-)$. The (un-normalized) QD eigenstate is

$$|\psi_m\rangle = \begin{bmatrix} e^{im\varphi}\left(\frac{J_m(k_+\rho)}{J_m(k_+R)} - \frac{J_m(k_-\rho)}{J_m(k_-R)}\right) \\ Ce^{i(m-1)\varphi}\left(\frac{J_{m-1}(k_+\rho)}{J_{m-1}(k_+R)} - \frac{J_{m-1}(k_-\rho)}{J_{m-1}(k_-R)}\right) \end{bmatrix}, \tag{4}$$

where C is a constant.

Previous studies on the circular TI QD [40,47,49] based on the mode-matching method solve Eq. (3) numerically to obtain the edge-state spectrum. Reference [38] uses a trial wave function (which does not satisfy the hardwall boundary condition) to derive an explicit analytical expression that shows that the edge states are equidistant in energy with a level spacing $\propto 1/R$. Reference [40] derived an explicit analytical expression in the large-dot limit that confirms the equidistance and the $1/R$ scaling but leaves a proportionality factor undetermined. Here we consider $|k_\pm|R \gg 1$ and solve Eq. (3) inside the bulk gap up to the second order to obtain (see Appendix B for detailed derivations)

$$E_m = -\frac{D}{B}M + \frac{|A|\sqrt{B_+B_-}}{B}k_m + \frac{A^2}{2MR}k_m, \tag{5}$$

where $k_m \equiv (m-1/2)/R$. In the large-dot limit $R\to\infty$, the edge states with different m have degenerate energies $-DM/B$. The second term in Eq. (5), i.e., the first-order correction due to the finite size of the QD, lifts the degeneracy and leads to equidistant energy levels with a level spacing $\propto 1/R$. Interestingly, the third term in Eq. (5), i.e., the second-order finite-size correction, still preserves the equidistance of the edge states, although it changes the $1/R$ scaling of the level spacing. As shown in Fig. 1, inclusion of the second-order finite-size correction makes our analytical expression agree well with the exact numerical results. Similar energy spectrums have been obtained *numerically* for QDs on the surface of 3D TIs [39,64] and for 2D TI QDs [49]. Here the good agreement between our *analytical* expression Eq. (5) and the exact numerical results demonstrates that the equidistance of the edge states is robust against the finite-size effect of the QD.

Next, we discuss two issues: (i) the chiral symmetry of the QD energy spectrum and (ii) the minimal QD radius R_c that supports helical edge states inside the bulk gap $[-|M|, |M|]$. For (i), we define the transformation $\hat{\Gamma} = \hat{\theta}\hat{C}$ with operator $\hat{C}$ interchanging $|e\rangle$ and $|hh\rangle$. When $D = 0$, the Hamiltonian $\mathbf{H}$ has chiral symmetry [64–66]:

$$\hat{\Gamma}\mathbf{H}\hat{\Gamma}^{-1} = -\mathbf{H}.$$

For the TI QD, the hardwall leaves the chiral symmetry intact, i.e., given a QD eigenstate $|\psi_m\rangle = [e^{im\varphi}F_1(\rho), e^{i(m-1)\varphi}F_2(\rho)]^T$ with eigenvalue E_m, the state $|\psi_{1-m}\rangle \equiv \hat{\Gamma}|\psi_m\rangle = [e^{i(1-m)\varphi}F_2^*(\rho), e^{i(-m)\varphi}F_1^*(\rho)]^T$ is also a QD eigenstate with energy $E_{1-m} = -E_m$. This chiral symmetry at $D = 0$ is obeyed by our analytical expression Eq. (5).

For (ii), according to Eq. (5), decreasing the QD radius shifts the edge-state energy E_m towards $-M$ (M) when $m \leqslant 0$ ($m \geqslant 1$), so the critical radius (denoted by R_m) for E_m to move outside the bulk gap can be estimated from $E_m = M$ ($E_m = -M$). For a more rigorous treatment, we determine R_m by solving Eq. (3) at $E = \pm M$ for R. In general, this

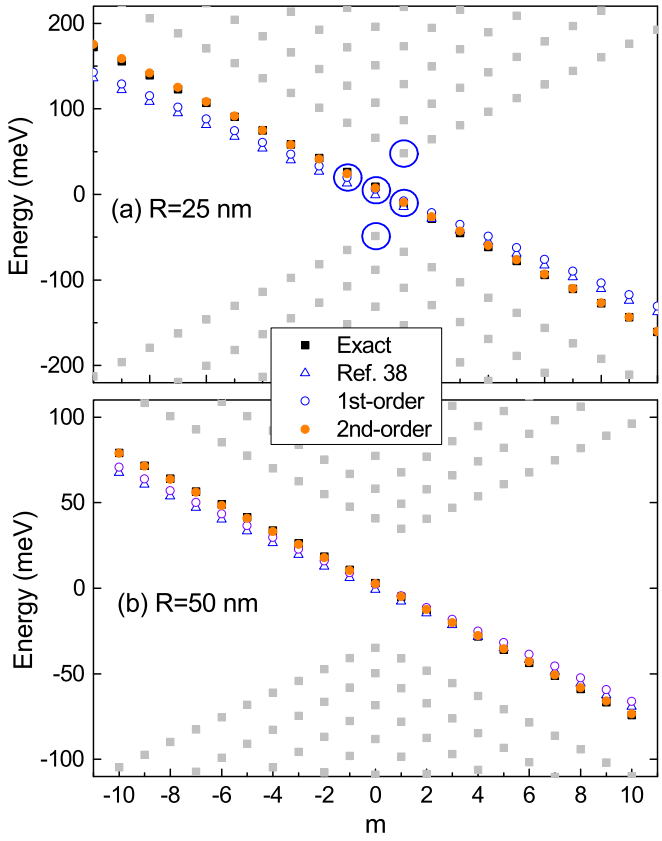

FIG. 1. Energy spectra of the TI QD with different radii: filled squares (gray for bulk states and black for edge states) for numerical results, blue triangles for analytical expression in Ref. [38], and empty (filled) circles for Eq. (5) up to the first (second) order of $1/R$. Other parameters are $A = -342$ meV nm, $B = -169$ meV nm^2, $D = 5.14$ meV nm^2, and $M = -30$ meV.

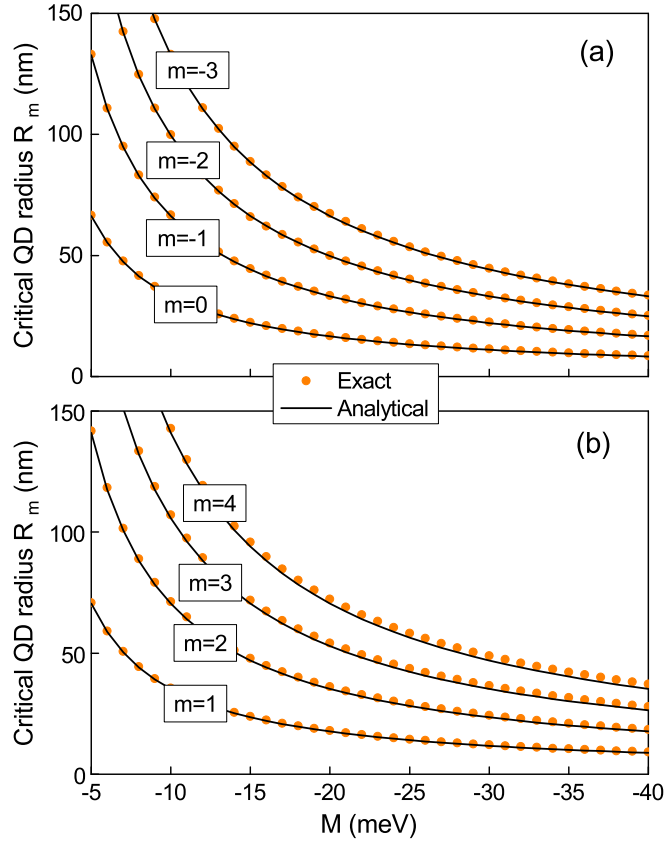

FIG. 2. Critical QD radius R_m for the existence of edge states $|\psi_m\rangle$ inside the bulk gap: (a) $m \leqslant 0$ and (b) $m \geqslant 1$. Symbols for exact numerical results and lines for analytical expression Eq. (6). Other parameters are the same as Fig. 1.

leads to a transcendental equation for R (see Appendix C for details). When $A^2 \gg 4BM$, we have an explicit analytical solution

$$R_m \approx \begin{cases} m\frac{|A|}{|M|}\sqrt{\frac{B_-}{B_+}} & (m \geqslant 1), \\ (|m|+1)\frac{|A|}{|M|}\sqrt{\frac{B_+}{B_-}} & (m \leqslant 0), \end{cases} \tag{6}$$

which obeys the chiral symmetry $R_{1-m} = R_m$ and agrees well with the numerical results in Fig. 2. The critical radius is

$$R_c \equiv \min_m R_m \approx |\frac{A}{M}|\sqrt{\frac{B_+}{B_-}}.$$

This suggests that a large nontrivial gap $|M|$ protects the existence of the edge states against decreasing QD size.

III. SUPPRESSED STARK SHIFT OF EDGE STATES IN TI QDS

For clarity, we use $E_{m,\alpha}$ and $|\psi_{m,\alpha}\rangle$ to label the eigenvalues and eigenstates of the circular TI QD, where α labels the different eigenstates with the same m (cf. Fig. 1). We characterize the stability of the (m,α)th energy level against electrical perturbations by its Stark shift $\Delta E_{m,\alpha}$ caused by an in-plane electric field F, whose direction is defined as the x axis. The presence of this electric field breaks the circular symmetry of the TI QD and hence makes the numerical calculation of $\Delta E_{m,\alpha}$ computationally expensive. Fortunately, the Stark shift caused by a *weak* electric field can be calculated reliably from the perturbation theory. Due to the circular symmetry of the QD in the absence of the electric field, the first-order contribution $eF\langle\psi_{m,\alpha}|x|\psi_{m,\alpha}\rangle$ to $\Delta E_{m,\alpha}$ vanishes. Thus we use the second-order perturbation theory to obtain $\Delta E_{m,\alpha} = \chi_{m,\alpha}F^2/2$, where

$$\chi_{m,\alpha} = 2e^2 \sum_\beta \left(\frac{|\langle\psi_{m-1,\beta}|x|\psi_{m,\alpha}\rangle|^2}{E_{m,\alpha} - E_{m-1,\beta}} + \frac{|\langle\psi_{m+1,\beta}|x|\psi_{m,\alpha}\rangle|^2}{E_{m,\alpha} - E_{m+1,\beta}} \right). \tag{7}$$

Here $E_{m,\alpha}$ and $|\psi_{m,\alpha}\rangle$ in Eq. (7) refer to the eigenenergies and eigenstates of the circular QD in the *absence* of the electric field. We call $\chi_{m,\alpha}$ the susceptibility of the (m,α)th energy level: the smaller $|\chi_{m,\alpha}|$, the more stable the energy level against the electric perturbations. We use two different methods to calculate $\{E_{m,\alpha}\}$ and $\{|\psi_{m,\alpha}\rangle\}$ and hence $\chi_{m,\alpha}$: (i) The mode-matching method (as outlined in the previous section), where $\{E_{m,\alpha}\}$ are obtained by solving the transcendental equation [Eq. (3)] numerically, while $\{|\psi_{m,\alpha}\rangle\}$ are given by Eq. (4). In solving Eq. (3), we have used a sufficiently high numerical precision to ensure accuracy of the resulting

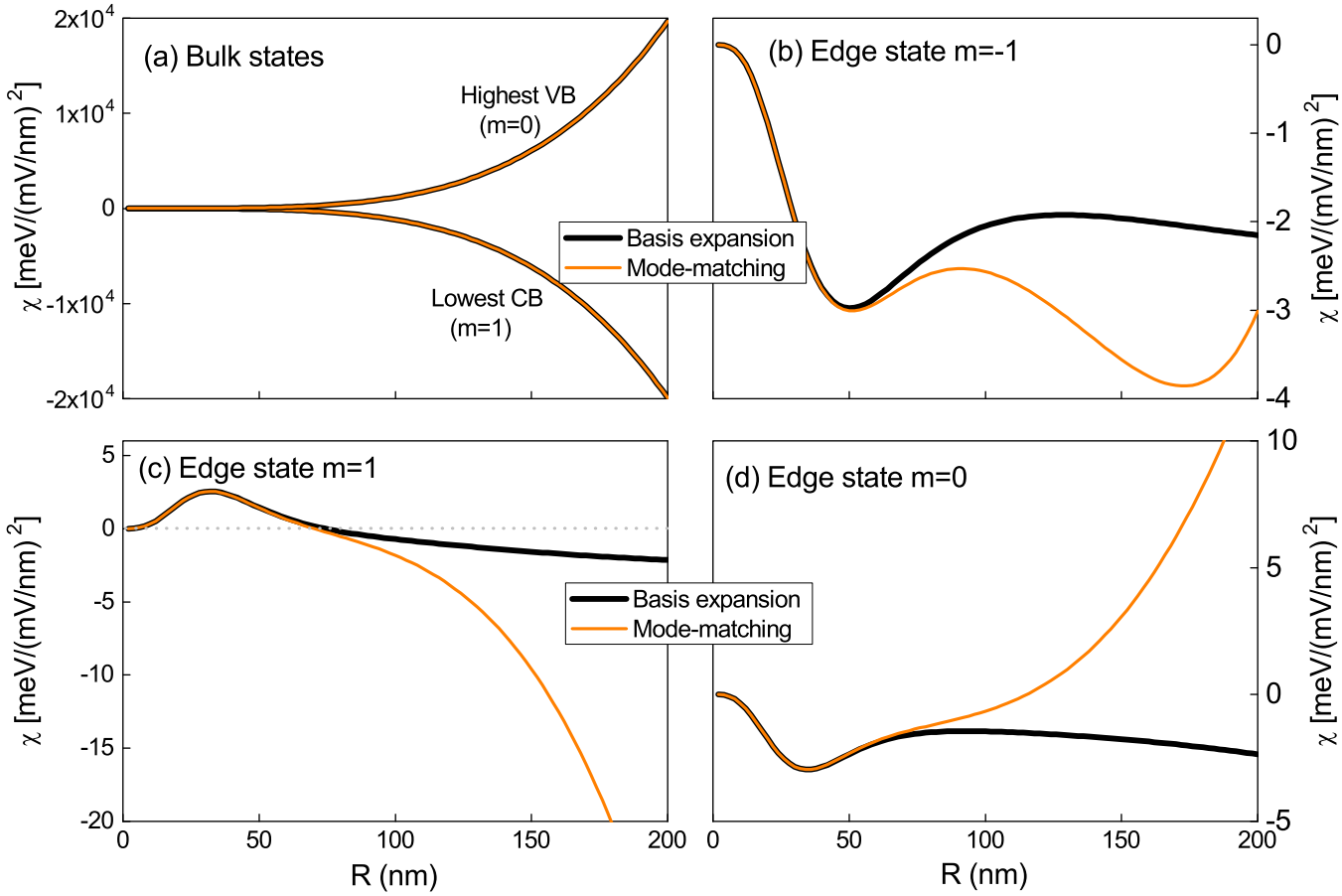

FIG. 3. Susceptibility of some QD eigenstates (as enclosed by the blue circles in Fig. 1) from the mode-matching method (black lines) and the basis-function expansion method with $n_c = 2000$ (orange lines). (a) The lowest bulk state in the conduction band ($m = 1$) and the highest bulk state in the valence band ($m = 0$). (b) $m = -1$ edge state; (c) $m = 1$ edge state, and (d) $m = 0$ edge state.

susceptibility $\chi_{m,\alpha}$ from Eq. (7). (ii) A basis expansion method which introduces an orthonormal, complete basis set and then diagonalizes the Hamiltonian matrix under this basis set (see Appendix D for details). If we use n_c basis functions, then the 2×2 spin-up Hamiltonian $\mathbf{H}$ of the TI QD becomes a $2n_c \times 2n_c$ matrix.

In Fig. 3, we plot the susceptibility of some typical QD eigenstates [indicated by the circles in Fig. 1(a)]. We observe two important features. First, the edge states are much more stable than the bulk states, e.g., $|\chi|$ for the lowest conduction band (highest valence band) is larger than that of the edge states by *4 orders of magnitude*. In particular, the $m = 1$ edge state has a vanishing susceptibility at $R \approx 70$ nm. Second, the mode-matching method and the basis function expansion method with $n_c = 2000$ give identical results for the bulk states [Fig. 3(a)], but they tend to differ strongly for the edge states [Figs. 3(b)–3(d)] when the QD radius increases. Since the results from the mode-matching method are numerically precise, the good agreement in Fig. 3(a) suggests that the basis function expansion method *converges well* at $n_c = 2000$ for the bulk states, while the large discrepancy in Figs. 3(b) and 3(d) indicates that the basis function expansion method is *far from convergence* at $n_c = 2000$ for the edge states. In principle, convergence can always be achieved by using a sufficiently large n_c. In practice, however, further increasing n_c is challenging since the computational cost of diagonalizing a $2n_c \times 2n_c$ matrix increases as $O(n_c^3)$. Due to this slow convergence, our previous study [59] fails to give quantitative results for the stability of edge states in relatively large TI QDs.

To understand the origin for these features, we take the susceptibility of the $m = 1$ edge state as an example and analyze the individual contributions. For convenience, we let $\alpha = 0$ for the edge states, $\alpha = 1, 2, \ldots$ for the bulk states in the conduction band with increasing energy, and $\alpha = -1, -2, \ldots$ for the bulk states in the valence band with decreasing energy. According to Eq. (7), only the $m = 0$ and $m = 2$ eigenstates contribute to the susceptibility $\chi_{1,0}$ of the $m = 1$ edge state:

$$\chi_{1,0} = 2e^2 \sum_{\beta=\pm1,\pm2,\cdots} \left(\frac{|\langle\psi_{0,\beta}|x|\psi_{1,0}\rangle|^2}{E_{1,0} - E_{0,\beta}} + \frac{|\langle\psi_{2,\beta}|x|\psi_{1,0}\rangle|^2}{E_{1,0} - E_{2,\beta}} \right) + 2e^2 \left(\frac{|\langle\psi_{0,0}|x|\psi_{1,0}\rangle|^2}{E_{1,0} - E_{0,0}} + \frac{|\langle\psi_{2,0}|x|\psi_{1,0}\rangle|^2}{E_{1,0} - E_{2,0}} \right).$$

The energies of these contributing states and those of the $m = 1$ edge state are shown in Fig. 4(a). The contributing states make pairs (as labeled by 0,1,2, and $1', 2', \ldots$). Each pair consists of one state above $E_{1,0}$ and one state below $E_{1,0}$. Except for pair 0, all the other pairs consist of bulk states. Since $|\psi_{1,0}\rangle$ is spatially separated from the bulk states, the overlap integrals $\langle\psi_{2,\beta}|x|\psi_{1,0}\rangle$ and $\langle\psi_{0,\beta}|x|\psi_{1,0}\rangle$ are small, especially for large QDs. As a result, the contribution from

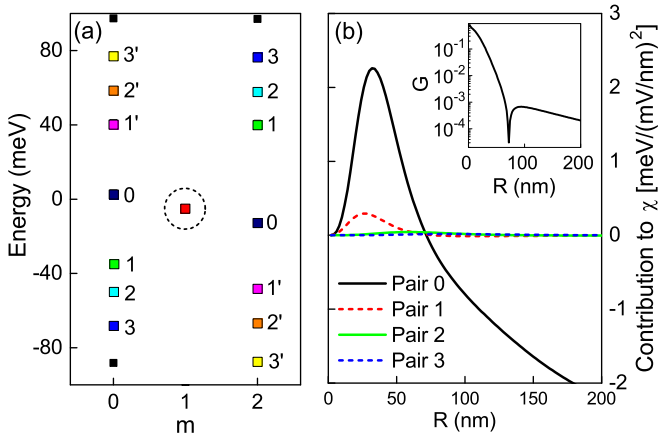

FIG. 4. (a) Energy levels of the $m = 0$ and $m = 2$ eigenstates for the $R = 50$ nm TI QD. These states make pairs, labeled by $0, 1, 2, \ldots$ and $1', 2', 3', \ldots$. (b) Contributions from each pair to the susceptibility of the $m = 1$ edge state (dashed circle). The inset shows the cancellation factor G for pair 0.

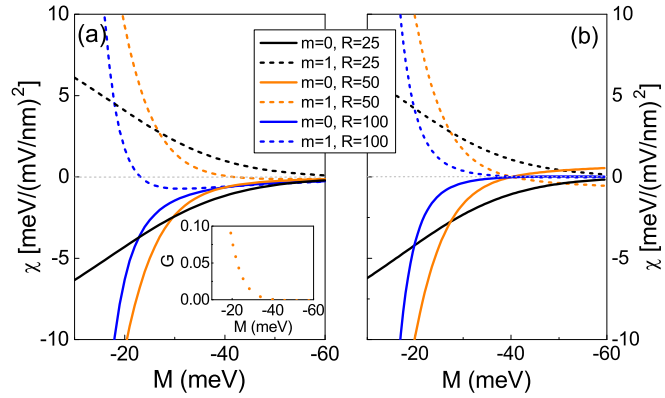

FIG. 5. Susceptibility of different edge states as functions of M for (a) $D = 5.14$ meV nm^2 and (b) $D = 0$. The unit of the QD radius R is nanometers. Other parameters are the same as Fig. 1. The inset shows the cancellation factor for pair 0 in the susceptibility of the $m = 1$ edge state at $R = 50$ nm.

the bulk states to $\chi_{1,0}$ is suppressed in relatively large QDs [see Fig. 4(b)] and the dominant contribution comes from pair 0, i.e., the two neighboring edge states:

$$\chi_{1,0} \approx 2e^2\left(\frac{|\langle\psi_{0,0}|x|\psi_{1,0}\rangle|^2}{E_{1,0}-E_{0,0}} - \frac{|\langle\psi_{2,0}|x|\psi_{1,0}\rangle|^2}{E_{2,0}-E_{1,0}}\right).$$

Since the edge states are equidistant, i.e., $E_{1,0} - E_{0,0} \approx E_{2,0} - E_{1,0}$, the first term and the second term tend to cancel each other. To investigate this cancellation in more detail, we define the cancellation factor G as the sum of both terms divided by the first term. As shown in Fig. 4(b), G decreases rapidly to $\sim 10^{-4}$ with increasing QD radius. This nearly complete cancellation originates from the equidistance of the edge states and is responsible for strong stability of the edge states compared with the bulk states. As a consequence of this cancellation, an accurate calculation of the edge-state susceptibility requires a much higher numerical precision for $\{E_{m,\alpha}\}$ and $\{|\psi_{m,\alpha}\rangle\}$ compared with the calculation of the bulk-state susceptibility. In the mode-matching method, increasing the number n_c of basis functions leads to slow improvement of the numerical precision but rapid increase of the computational cost as $O(n_c^3)$. This makes it challenging to calculate the edge-state susceptibility reliably with the basis expansion method.

Next we discuss the dependence of the susceptibilities on the QD radius and the nontrivial gap $|M|$. As shown in Fig. 3(a), the susceptibility of the bulk states increases rapidly with the QD radius due to the increase of the overlap integral [i.e., numerators in Eq. (7)] and decrease of the level spacing [i.e., denominators in Eq. (7)]. By contrast, the susceptibility of the edge states shows complicated dependences on the QD radius. This is because increasing the QD radius leads to two competing effects. First, it decreases the level spacing and hence tends to increase the susceptibility. Second, it makes the edge states more equidistant and leads to better cancellation [see the inset of Fig. 4(b)].

As shown in Fig. 5(a), increasing the nontrivial gap $|M|$ tends to enhance the stability of the edge states. The physical origin is that increasing $|M|$ increases $|k_+|$ inside the bulk gap to make $|k_\pm R| \gg 1$ and hence Eq. (5) is better satisfied, so that the edge states become more equidistant. This in turn increases the degree of cancellation of pair contributions [see the inset of Fig. 5(a)]. In other words, increasing $|M|$ improves the equidistance of the edge states without changing their energy separation, so it further stabilizes the edge states.

An interesting issue is the chiral symmetry of the susceptibilities at $D = 0$. In this case, the energy and wave function of (m, α) and $(1 - m, -\alpha)$ are connected by $E_{1-m,-\alpha} = -E_{m,\alpha}$ and $|\psi_{1-m,-\alpha}\rangle = \hat{\Gamma}|\psi_{m,\alpha}\rangle$, so

$$\langle\psi_{-m,-\beta}|x|\psi_{1-m,-\alpha}\rangle = \langle\psi_{m+1,\beta}|x|\psi_{m,\alpha}\rangle^*,$$
$$\langle\psi_{2-m,-\beta}|x|\psi_{1-m,-\alpha}\rangle = \langle\psi_{m-1,\beta}|x|\psi_{m,\alpha}\rangle^*.$$

Substituting into Eq. (7) gives

$$\chi_{1-m,-\alpha} = -\chi_{m,\alpha},$$

as confirmed in Fig. 5(b). Physically, the chiral symmetry of the susceptibility originates from the preservation of the chiral symmetry under the in-plane electric field.

Finally, we discuss possible generalization of the strong stability of the edge states to noncircular TI QDs. Physically, suppression of the Stark shift of an edge state $|\psi_{m,0}\rangle$ due to an in-plane electric field (whose direction is defined as the x axis) in a noncircular TI QD requires two conditions: (i) The vanishing first-order contribution $eF\langle\psi_{m,0}|x|\psi_{m,0}\rangle$ to the Stark shift. This requires the TI QD to possess a symmetry that makes $\langle\psi_{m,0}|x|\psi_{m,0}\rangle = 0$, e.g., spatial inversion symmetry or mirror symmetry about the yz plane—the plane perpendicular to the electric field. In other words, the spatial inversion symmetry could stabilize the edge states against electric fields along any direction, while mirror symmetry could stabilize the edge states against electric fields perpendicular to the mirror plane. (ii) Linear dispersion of the one-dimensional edge channel spectrum $E(k_x)$, as proved recently by Entin *et al.* [67] for the BHZ model. For large TI QDs such that the edge states on opposite QD edges have negligible overlap, the discrete edge-state spectrum $\{E_m\}$ is obtained from $E(k_x)$ by quantizing the continuous momentum

k_x into discrete momentum $k_m \approx 2m\pi/L$ ($m \in \mathbb{Z}$) (due to the periodic boundary condition along the QD edge of total length L [41]), i.e., $E_m = E(k_m)$. Since k_m are equidistant, the edge-state spectrum $\{E_m\}$ will also be equidistant if the dispersion $E(k_x)$ is linear. In this case, the spatial separation of the edge states from the bulk states suppresses the second-order contributions from the bulk states to the Stark shift of the edge state. The equidistant nature of the edge states further suppresses the second-order contributions from other edge states. Therefore, under conditions (i) and (ii), we expect the strong stability of the edge states against electric field perturbations to be a general feature for relatively large TI QDs.

IV. CONCLUSION

We have studied the stability of the helical edge states in circular two-dimensional topological-insulator (TI) quantum dots (QDs). With the Stark shift of each QD eigenstate as a figure of merit for this stability (the smaller the Stark shift, the more stable the state), we have shown that the Stark shifts of the edge states are typically 4 orders of magnitude smaller than those of the normal bulk states (that localize at the interior of the QD). We have also identified the spatial separation of the edge states from the bulk states and the equidistance of the edge states as key ingredients for this strong stability. Since both ingredients also exist even in noncircular QDs, we expect the same physical mechanism to stabilize the edge states of noncircular TI QDs. This finding may be relevant to the applications of these edge states in various quantum technologies.

ACKNOWLEDGMENTS

This work was supported by the National Key R&D Program of China (Grant No. 2017YFA0303400), the MOST of China (Grant No. 2014CB848700), the NSFC (Grants No. 11774021, No. 11322542, and No. 11504018), and the NSFC program for "Scientific Research Center" (Grant No. U1530401). We acknowledge computational support from the Beijing Computational Science Research Center (CSRC).

APPENDIX A: MODE-MATCHING APPROACH TO TI QUANTUM DOT

We work in the polar coordinate (ρ, φ). For cylinder functions $Z_m(x)$ of integer order $m \in \mathbb{Z}$, such as the Bessel function $J_m(x)$ and Neumann function $N_m(x)$, we have

$$\hat{k}^2[e^{im\varphi} Z_m(k\rho)] = k^2[e^{im\varphi} Z_m(k\rho)], \tag{A1a}$$

$$\hat{k}_\pm[e^{im\varphi} Z_m(k\rho)] = \pm ik[e^{i(m\pm1)\varphi} Z_{m\pm1}(k\rho)], \tag{A1b}$$

so the bulk eigenstate that remains finite at $\rho = 0$ can be written as $|\Phi_m\rangle = [\alpha e^{im\varphi} J_m(k\rho), \beta e^{i(m-1)\varphi} J_{m-1}(k\rho)]^T$, where α, β, k are unknown numbers. Substituting $|\Phi_m\rangle$ into Eq. (2) gives

$$\begin{bmatrix} M - B_+k^2 & iAk \\ -iAk & -M + B_-k^2 \end{bmatrix} \begin{bmatrix} \alpha \\ \beta \end{bmatrix} = E \begin{bmatrix} \alpha \\ \beta \end{bmatrix}. \tag{A2}$$

Given an energy E, in order for Eq. (A2) to have nontrivial solutions for (k, α, β), the determinant must vanish:

$$\det \begin{bmatrix} M - E - B_+k^2 & iAk \\ -iAk & -M - E + B_-k^2 \end{bmatrix} = 0.$$

This leads to $k^4 + 2Fk^2 + m_+m_- = 0$, where $m_\pm \equiv (M \mp E)/B_\pm$, and $F \equiv A^2/(2B_+B_-) - (m_+ + m_-)/2$. This equation has four solutions for (k, α, β), as denoted by $(k_\pm, \alpha_\pm, \beta_\pm)$ and $(-k_\pm, \alpha_\pm, -\beta_\pm)$, where $k_\pm = \sqrt{-F \pm \sqrt{F^2 - m_+m_-}}$ and

$$\frac{\alpha_\pm}{\beta_\pm} = \frac{i(A/B_+)k_\pm}{k_\pm^2 - m_+} = \frac{k_\pm^2 - m_-}{i(A/B_-)k_\pm}. \tag{A3}$$

The bulk eigenstates associated with $(k_\pm, \alpha_\pm, \beta_\pm)$ are

$$|\Phi_m^{(\pm)}\rangle = \begin{bmatrix} \alpha_\pm e^{im\varphi} J_m(k_\pm\rho) \\ \beta_\pm e^{i(m-1)\varphi} J_{m-1}(k_\pm\rho) \end{bmatrix}.$$

Following Ref. [15], we consider $B_+B_- > 0$ and $A^2 > 4BM > 0$. Since $J_m(-z) = (-1)^m J_m(z)$, the bulk eigenstates associated with $(-k_\pm, \alpha_\pm, -\beta_\pm)$ are $(-1)^m|\Phi_m^{(\pm)}\rangle$. Therefore, there are only two independent bulk eigenstates $|\Phi_m^{(\pm)}\rangle$. The QD eigenstate is their linear combination: $|\psi_m\rangle = c_+|\Phi_m^{(+)}\rangle + c_-|\Phi_m^{(-)}\rangle$. Imposing the hardwall boundary condition $\psi_m|_{\rho=R} = 0$ at the QD edge gives

$$\begin{bmatrix} \alpha_+ J_m(k_+R) & \alpha_- J_m(k_-R) \\ \beta_+ J_{m-1}(k_+R) & \beta_- J_{m-1}(k_-R) \end{bmatrix} \begin{bmatrix} c_+ \\ c_- \end{bmatrix} = 0. \tag{A4}$$

To have nontrivial solutions, the determinant must vanish:

$$\frac{\beta_+}{\alpha_+} \frac{J_{m-1}(k_+R)}{J_m(k_+R)} = \frac{\beta_-}{\alpha_-} \frac{J_{m-1}(k_-R)}{J_m(k_-R)} \equiv C.$$

This condition, together with Eq. (A3), leads to the transcendental equation Eq. (3) that determines the allowed energy. Equation (A4) also determines c_+/c_- and hence the eigenstate in Eq. (4).

APPENDIX B: ANALYTICAL EXPRESSION FOR EDGE-STATE ENERGY IN LARGE QUANTUM DOTS

For the energy inside the bulk gap, we have $k_\pm = i\kappa_\pm$, so Eq. (3) becomes

$$g(E) = \mathbb{J}_m(E),$$

where

$$g(E) \equiv \frac{\kappa_-(m_+ + \kappa_+^2)}{\kappa_+(m_+ + \kappa_-^2)} = \frac{\kappa_+(m_- + \kappa_-^2)}{\kappa_-(m_- + \kappa_+^2)}$$

and

$$\mathbb{J}_m(E) = \frac{I_m(\kappa_+R)/I_{m-1}(\kappa_+R)}{I_m(\kappa_-R)/I_{m-1}(\kappa_-R)},$$

with $I_m(x)$ the modified Bessel function of the mth order. We can express $m_\pm$ in terms of $\mathbb{J}_m$ and $\kappa_\pm$:

$$m_+ = -\kappa_+\kappa_- \frac{\mathbb{J}_m\kappa_- - \kappa_+}{\mathbb{J}_m\kappa_+ - \kappa_-},$$

$$m_- = -\kappa_+\kappa_- \frac{\mathbb{J}_m\kappa_+ - \kappa_-}{\mathbb{J}_m\kappa_- - \kappa_+}.$$

The second equation can also be obtained from the first equation by using $\kappa_+^2\kappa_-^2 = m_+m_-$. Subtracting the two equations gives

$$E = -\frac{MD}{B} + \frac{B_+B_-}{2B}\kappa_+\kappa_-\left(\frac{\mathbb{J}_m\kappa_- - \kappa_+}{\mathbb{J}_m\kappa_+ - \kappa_-} - \frac{\mathbb{J}_m\kappa_+ - \kappa_-}{\mathbb{J}_m\kappa_- - \kappa_+}\right). \tag{B1}$$

For $\kappa_- R \gg 1$, we can use $[I_m(x)/I_{m-1}(x)]_{x\gg1} \approx 1 - (m - 1/2)/x + (m^2/2 - m + 3/8)/x^2$ to obtain $\mathbb{J}_m = 1 + a_1/R + a_2/R^2$ up to $O(1/R^2)$, where

$$a_1 = -\frac{\kappa_- - \kappa_+}{2\kappa_+\kappa_-}(2m-1),$$

$$a_2 = (2m-1)(\kappa_- - \kappa_+)\frac{(2m-3)\kappa_- - (2m+1)\kappa_+}{8(\kappa_+\kappa_-)^2}.$$

Then we can expand Eq. (B1) up to $1/R^2$ as

$$E \approx -\frac{MD}{B} + \frac{B_+B_-}{2B}(2m-1)(\kappa_- + \kappa_+)\left(\frac{1}{R} + \frac{\kappa_- + \kappa_+}{2\kappa_-\kappa_+R^2}\right), \tag{B2}$$

where

$$\kappa_+\kappa_- = \sqrt{m_+m_-} = \sqrt{\frac{M^2 - E^2}{B_+B_-}}, \tag{B3}$$

$$\kappa_+ + \kappa_- = \sqrt{2F + 2\sqrt{m_+m_-}} = \sqrt{2F + 2\sqrt{\frac{M^2 - E^2}{B_+B_-}}}. \tag{B4}$$

Next we solve Eq. (B2) perturbatively up to $O(1/R^2)$. For the zeroth order, Eq. (B2) immediately gives the edge-state energy $E^{(0)} = -MD/B$ and hence $(\kappa_+\kappa_-)^{(0)} = M/B$, $(\kappa_+ + \kappa_-)^{(0)} = |A|/\sqrt{B_+B_-}$. For the first order, we can replace $\kappa_+ + \kappa_-$ in Eq. (B2) with $(\kappa_+ + \kappa_-)^{(0)}$ and neglect second- and higher-order terms in Eq. (B2) to obtain

$$E^{(1)} = -\frac{MD}{B} + \frac{|A|\sqrt{B_+B_-}}{B}\frac{m - 1/2}{R}.$$

Next we replace E with $E^{(1)}$ in Eq. (B4) to obtain $(\kappa_+ + \kappa_-)^{(1)}$, which turns out to be identical to $(\kappa_+ + \kappa_-)^{(0)}$. For the second order, we replace $\kappa_- + \kappa_+$ in Eq. (B2) with $(\kappa_+ + \kappa_-)^{(1)}$ and neglect third- and higher-order terms in Eq. (B2) to obtain

$$E^{(2)} = -\frac{D}{B}M + \frac{|A|\sqrt{B_+B_-}}{B}\frac{m - 1/2}{R} + \frac{A^2}{2MR}\frac{m - 1/2}{R}.$$

Therefore, up to the second order of $1/R$, the edge-state spectrum is still equidistant. This interesting feature originates from $(\kappa_+ + \kappa_-)^{(1)} = (\kappa_+ + \kappa_-)^{(0)}$, i.e., the vanishing first-order derivative of $\kappa_+ + \kappa_-$, as a function of E at $E = E^{(0)}$.

APPENDIX C: CONDITIONS FOR EXISTENCE OF EDGE STATES IN THE BULK GAP

For the energy inside the bulk gap, we have $k_\pm = i\kappa_\pm$. According to Eq. (5), when $m \geqslant 1$ ($m \leqslant 0$), decreasing R shifts E_m towards M ($-M$), so the critical radius R_m is determined by $E_m = M$ ($E_m = -M$) as

$$R_m = \begin{cases} (m - \frac{1}{2})\frac{|A|}{|M|}\sqrt{\frac{B_-}{B_+}} & (m \geqslant 1), \\ (|m| + \frac{1}{2})\frac{|A|}{|M|}\sqrt{\frac{B_+}{B_-}} & (m \leqslant 0). \end{cases} \tag{C1}$$

However, Eq. (5) is valid only when $|k_+|R \gg 1$, while the critical QD radius corresponds to $|k_+| \to 0$, so Eq. (C1) only serves as a rough estimate.

For a rigorous treatment, we should determine R_m by solving Eq. (3) at $E = \pm M$ for R. When $E \to \pm M$, we have $\kappa_+ \to 0$, $\kappa_- = \sqrt{2F(\pm M)}$,

$$\mathbb{J}_m(\pm M) = \frac{1}{c_m(\pm M)}\begin{cases} \frac{\kappa_+ R}{2m} & (m \geqslant 1), \\ \frac{2(|m|+1)}{\kappa_+ R} & (m \leqslant 0), \end{cases}$$

and

$$g(\pm M) = \left[\left(1 + \frac{B_\mp F(\pm M)}{M}\right)\frac{\kappa_+}{\sqrt{2F(\pm M)}}\right]^{\pm 1},$$

where $c_m(E) \equiv I_m(\kappa_- R)/I_{m-1}(\kappa_- R)$. At $E = M$, Eq. (3) has a solution for R only when $m \geqslant 1$, i.e., Eq. (3) at $E = M$ determines the critical radius for edge states with $m \geqslant 1$:

$$\frac{\sqrt{2F(M)}R}{c_m(M)} = 2m\left(1 + \frac{B_- F(M)}{M}\right). \tag{C2}$$

At $E = -M$, Eq. (3) has solution for R only when $m \leqslant 0$, i.e., Eq. (3) at $E = -M$ determines the critical radius for edge states with $m \leqslant 0$:

$$c_m(-M)\sqrt{2F(-M)}R = 2(|m| + 1)\left[1 + \frac{B_+}{M}F(-M)\right]. \tag{C3}$$

Equations (C2) and (C3) are complicated nonlinear equations for R since $c_m(\pm M)$ depends on R in a complicated way. When $A^2 \gg 4BM$, we have $c_m(\pm M) \approx 1$ and $F(\pm M) \approx A^2/(2B_+B_-) \gg M/B_\mp$, and thus we obtain Eq. (6).

APPENDIX D: BASIS FUNCTION EXPANSION METHOD FOR TI QUANTUM DOTS

The idea is to expand the QD eigenstates in an orthonormal complete basis set that obeys the same hardwall boundary condition (i.e., the wave function must vanish at $\rho = R$) as the QD eigenstates. Since $\hat{k}^2$ appears in the Hamiltonian $\mathbf{H}$, it is natural to choose the eigenstates (with eigenvalue k_{mn}^2)

$$\Phi_{mn}(\rho, \varphi) \equiv \frac{e^{im\varphi}}{\sqrt{2\pi}}\frac{J_m(k_{mn}\rho)}{\mathbb{N}_{mn}}$$

of the Hermitian operator $\hat{k}^2$ as the orthonormal basis, where $m \in \mathbb{Z}$, k_{mn} is the nth zero ($n = 1, 2, \dots$) of the mth-order Bessel function $J_m(kR)$ as a function of k, and $\mathbb{N}_{mn} \equiv |RJ_{|m|+1}(k_{m,n}R)|/\sqrt{2}$ is a numerical factor to ensure the orthonormalization $\langle\Phi_{mn}|\Phi_{m'n'}\rangle = \delta_{mm'}\delta_{nn'}$. Any wave function in the xy plane that obeys the hardwall boundary condition at $\rho = R$ can be expanded into a linear combination of $\{\Phi_{mn}\}$.

The spin-up eigenstate can be expanded as

$$|\psi\rangle = \sum_{mn}\begin{bmatrix} C_{mn}^{(1)}\Phi_{mn}(\rho, \varphi) \\ C_{mn}^{(2)}\Phi_{mn}(\rho, \varphi) \end{bmatrix},$$

and then Eq. (2) becomes an eigenvalue equation $\sum_{j',m',n'}\langle\Phi_{mn}|\hat{H}_{jj'}|\Phi_{m'n'}\rangle C^{(j')}_{m'n'} = EC^{(j)}_{mn}$, where $\hat{H}_{jj'}$ is the (j, j') matrix element of $\mathbf{H}$. Using Eq. (A1) gives

$$\left\langle\Phi^{(m)}_n\middle|\hat{H}_{11}\middle|\Phi^{(m')}_{n'}\right\rangle = \delta_{m,m'}\delta_{n,n'}\left(M - B_+k^2_{mn}\right),$$
$$\left\langle\Phi^{(m)}_n\middle|\hat{H}_{22}\middle|\Phi^{(m')}_{n'}\right\rangle = \delta_{m,m'}\delta_{n,n'}\left(-M + B_-k^2_{mn}\right),$$
$$\left\langle\Phi^{(m)}_n\middle|\hat{H}_{12}\middle|\Phi^{(m')}_{n'}\right\rangle = \delta_{m,m'+1}iAk_{m'n'}\frac{\int_0^R J_m(k_{mn}\rho)J_m(k_{m'n'}\rho)\rho d\rho}{\mathbb{N}_{mn}\mathbb{N}_{m'n'}}.$$

This suggests that m is a good quantum number, i.e., the spin-up eigenstate can be labeled by a single m:

$$|\psi_m\rangle = \begin{bmatrix} e^{im\varphi}F_1(\rho) \\ e^{i(m-1)\varphi}F_2(\rho)\end{bmatrix} = \sum_n \begin{bmatrix} C^{(1)}_{mn}\Phi_{mn}(\rho,\varphi) \\ C^{(2)}_{m-1,n}\Phi_{m-1,n}(\rho,\varphi)\end{bmatrix},$$

and the eigenvalue equation simplifies to $\sum_{j',n'}\langle\Phi_{m_jn}|\hat{H}_{jj'}|\Phi_{m_{j'}n'}\rangle C^{(j')}_{m_{j'}n'} = EC^{(j)}_{m_jn}$, where $m_1 \equiv m$ and $m_2 \equiv m-1$. With the sum over n truncated to $n \leqslant n_c$, it becomes an eigenvalue problem for a $2n_c \times 2n_c$ Hermitian matrix. We should choose a sufficiently large cutoff n_c to ensure the convergence.

[1] C. L. Kane and E. J. Mele, Phys. Rev. Lett. **95**, 226801 (2005).
[2] C. L. Kane and E. J. Mele, Phys. Rev. Lett. **95**, 146802 (2005).
[3] B. A. Bernevig and S.-C. Zhang, Phys. Rev. Lett. **96**, 106802 (2006).
[4] B. A. Bernevig, T. L. Hughes, and S.-C. Zhang, Science **314**, 1757 (2006).
[5] M. König, S. Wiedmann, C. Brüne, A. Roth, H. Buhmann, L. W. Molenkamp, X.-L. Qi, and S.-C. Zhang, Science **318**, 766 (2007).
[6] W. Yang, K. Chang, and S.-C. Zhang, Phys. Rev. Lett. **100**, 056602 (2008).
[7] M. Z. Hasan and C. L. Kane, Rev. Mod. Phys. **82**, 3045 (2010).
[8] X.-L. Qi and S.-C. Zhang, Rev. Mod. Phys. **83**, 1057 (2011).
[9] Y. Ando, J. Phys. Soc. Jpn. **82**, 102001 (2013).
[10] M. S. Miao, Q. Yan, C. G. Van de Walle, W. K. Lou, L. L. Li, and K. Chang, Phys. Rev. Lett. **109**, 186803 (2012).
[11] D. Zhang, W. Lou, M. Miao, S.-C. Zhang, and K. Chang, Phys. Rev. Lett. **111**, 156402 (2013).
[12] L. Shi, W. Lou, F. Cheng, Y. L. Zou, W. Yang, and K. Chang, Sci. Rep. **5**, 15266 (2015).
[13] C. Wu, B. A. Bernevig, and S.-C. Zhang, Phys. Rev. Lett. **96**, 106401 (2006).
[14] C. Xu and J. E. Moore, Phys. Rev. B **73**, 045322 (2006).
[15] B. Zhou, H.-Z. Lu, R.-L. Chu, S.-Q. Shen, and Q. Niu, Phys. Rev. Lett. **101**, 246807 (2008).
[16] J. Maciejko, C. Liu, Y. Oreg, X.-L. Qi, C. Wu, and S.-C. Zhang, Phys. Rev. Lett. **102**, 256803 (2009).
[17] G. Tkachov and E. M. Hankiewicz, Phys. Rev. Lett. **104**, 166803 (2010).
[18] J. C. Budich, F. Dolcini, P. Recher, and B. Trauzettel, Phys. Rev. Lett. **108**, 086602 (2012).
[19] A. Tadjine and C. Delerue, Phys. Rev. B **95**, 235426 (2017).
[20] M. Büttiker, Science **325**, 278 (2009).
[21] C. Liu, T. L. Hughes, X.-L. Qi, K. Wang, and S.-C. Zhang, Phys. Rev. Lett. **100**, 236601 (2008).
[22] M. König, H. Buhmann, L. W. Molenkamp, T. Hughes, C.-X. Liu, X.-L. Qi, and S.-C. Zhang, J. Phys. Soc. Jpn. **77**, 031007 (2008).
[23] A. Roth, C. Brüne, H. Buhmann, L. W. Molenkamp, J. Maciejko, X.-L. Qi, and S.-C. Zhang, Science **325**, 294 (2009).
[24] C. Brune, A. Roth, H. Buhmann, E. M. Hankiewicz, L. W. Molenkamp, J. Maciejko, X.-L. Qi, and S.-C. Zhang, Nat. Phys. **8**, 485 (2012).
[25] M. König, M. Baenninger, A. G. F. Garcia, N. Harjee, B. L. Pruitt, C. Ames, P. Leubner, C. Brüne, H. Buhmann, L. W. Molenkamp, and D. Goldhaber-Gordon, Phys. Rev. X **3**, 021003 (2013).
[26] I. Knez, R.-R. Du, and G. Sullivan, Phys. Rev. Lett. **107**, 136603 (2011).
[27] I. Knez, R.-R. Du, and G. Sullivan, Phys. Rev. Lett. **109**, 186603 (2012).
[28] K. Suzuki, Y. Harada, K. Onomitsu, and K. Muraki, Phys. Rev. B **87**, 235311 (2013).
[29] I. Knez, C. T. Rettner, S.-H. Yang, S. S. P. Parkin, L. Du, R.-R. Du, and G. Sullivan, Phys. Rev. Lett. **112**, 026602 (2014).
[30] P. Michetti and B. Trauzettel, Appl. Phys. Lett. **102**, 063503 (2013).
[31] H.-H. Fu, J.-H. Gao, and K.-L. Yao, Nanotechnology **25**, 225201 (2014).
[32] L. B. Zhang, K. Chang, X. C. Xie, H. Buhmann, and L. W. Molenkamp, New J. Phys. **12**, 083058 (2010).
[33] L. B. Zhang, F. Zhai, and K. Chang, Phys. Rev. B **81**, 235323 (2010).
[34] L. B. Zhang, F. Cheng, F. Zhai, and K. Chang, Phys. Rev. B **83**, 081402(R) (2011).
[35] L.-Z. Lin, F. Cheng, L. B. Zhang, D. Zhang, and W. Yang, Phys. Rev. B **87**, 245311 (2013).
[36] L.-Z. Lin, F. Cheng, D. Zhang, W.-K. Lou, and L.-B. Zhang, Solid State Commun. **161**, 34 (2013).
[37] P. Michetti and P. Recher, Phys. Rev. B **83**, 125420 (2011).
[38] K. Chang and W.-K. Lou, Phys. Rev. Lett. **106**, 206802 (2011).
[39] G. J. Ferreira and D. Loss, Phys. Rev. Lett. **111**, 106802 (2013).
[40] M. Pang and X. G. Wu, arXiv:1309.5559.
[41] J. Li, W.-K. Lou, D. Zhang, X.-J. Li, W. Yang, and K. Chang, Phys. Rev. B **90**, 115303 (2014).
[42] P. Potasz and J. Fernandez-Rossier, Nano Lett. **15**, 5799 (2015).
[43] Y. Xing, Z. L. Yang, Q. F. Sun, and J. Wang, Phys. Rev. B **90**, 075435 (2014).

[44] C. Ertler, M. Raith, and J. Fabian, Phys. Rev. B **89**, 075432 (2014).
[45] X. Xin and D. Zhou, Phys. Rev. B **91**, 165120 (2015).
[46] L. Jian and Z. Dong, Chin. Phys. Lett. **32**, 047303 (2015).
[47] A. Sukhanov, Physica B (Amsterdam, Neth.) **513**, 1 (2017).
[48] J. Li, D. Zhang, and J.-J. Zhu, Physica E (Amsterdam, Neth.) **93**, 58 (2017).
[49] D. R. Candido, M. E. Flatté, and J. C. Egues, Phys. Rev. Lett. **121**, 256804 (2018).
[50] D. Loss and D. P. DiVincenzo, Phys. Rev. A **57**, 120 (1998).
[51] L. kun Shi, K. Chang, and C.-P. Sun, arXiv:1601.04722.
[52] Z. Wu, L. Lin, W. Yang, D. Zhang, C. Shen, W. Lou, H. Yin, and K. Chang, RSC Adv. **7**, 30963 (2017).
[53] M. Kolodrubetz, B. M. Fregoso, and J. E. Moore, Phys. Rev. B **94**, 195124 (2016).
[54] H. Koochaki Kelardeh, V. Apalkov, and M. I. Stockman, Phys. Rev. B **96**, 075409 (2017).
[55] S. A. Oliaei Motlagh, J.-S. Wu, V. Apalkov, and M. I. Stockman, Phys. Rev. B **98**, 125410 (2018).
[56] S. A. Oliaei Motlagh, J.-S. Wu, V. Apalkov, and M. I. Stockman, Phys. Rev. B **98**, 081406 (2018).
[57] X. Hu and S. Das Sarma, Phys. Rev. Lett. **96**, 100501 (2006).
[58] W. Yang, W.-L. Ma, and R.-B. Liu, Rep. Prog. Phys. **80**, 016001 (2017).
[59] J.-X. Qu, S.-H. Zhang, D.-Y. Liu, P. Wang, and W. Yang, J. Appl. Phys. **122**, 034307 (2017).
[60] D. G. Rothe, R. W. Reinthaler, C.-X. Liu, L. W. Molenkamp, S.-C. Zhang, and E. M. Hankiewicz, New J. Phys. **12**, 065012 (2010).
[61] L.-K. Shi, S.-C. Zhang, and K. Chang, Phys. Rev. B **87**, 161115 (2013).
[62] D. Ferry and S. Goodnick, *Transport in Nanostructures* (Cambridge University Press, Cambridge, UK, 1997).
[63] E. Tsitsishvili, G. S. Lozano, and A. O. Gogolin, Phys. Rev. B **70**, 115316 (2004).
[64] B. Messias de Resende, F. C. de Lima, R. H. Miwa, E. Vernek, and G. J. Ferreira, Phys. Rev. B **96**, 161113 (2017).
[65] A. P. Schnyder, S. Ryu, A. Furusaki, and A. W. W. Ludwig, Phys. Rev. B **78**, 195125 (2008).
[66] S. Ryu, A. P. Schnyder, A. Furusaki, and A. W. W. Ludwig, New J. Phys. **12**, 065010 (2010).
[67] M. V. Entin, M. M. Mahmoodian, and L. I. Magarill, Europhys. Lett. **118**, 57002 (2017).